Nano Research 2016, 9(5): 1532–1542
DOI 10.1007/s12274-016-1049-2
Research Article
ISSN 1998-0124
CN 11-5974/O4

Probing the seeded protocol for high-concentration preparation of silver nanowires

Cheng Wang, Baisong Cheng, Haichuan Zhang, Pengbo Wan, Liang Luo (✉), Yun Kuang (✉), and Xiaoming Sun

State Key Laboratory of Chemical Resource Engineering, P.O. Box 98, Beijing University of Chemical Technology, Beijing 100029, China

Received: 8 January 2016
Revised: 1 February 2016
Accepted: 14 February 2016

KEYWORDS
silver nanowire,
seeded protocol,
nucleation,
large-scale

ABSTRACT

Mass production of high-quality silver nanowires (Ag NWs) is of significant importance because of its potential applications in flexible transparent conductive devices. Halogen ions have been widely used for the synthesis of Ag NWs; however, owing to the lack of a deep insight into heterogeneous nucleation processes, usually a trace feeding amount (e.g. $[Cl^-] < 0.25$ mM) is used, which in turn lowers the concentration of precursor ($[Ag^+]$). Here we systematically investigated the nucleation and growth behavior of Ag NWs and concluded that the number of heterogeneous nucleation sites was determined by the total surface area of AgCl seeds, which indicated a linear relationship between the concentrations of Ag^+ and Cl^- during precipitation. Based on this mechanism, we successfully produced high-quality Ag NWs with Ag^+ concentrations which were 20 times higher for a polyol system and 5 times higher for an aqueous system as compared to that in the previously reported strategies. Besides, by tailoring the heterogeneous nucleation sites by controlling the size of the AgCl seeds, the diameters of the final Ag NWs could be well controlled even at high Ag^+ concentration. Based on the mechanistic understandings, this synthetic strategy could be extended to other AgX-seeds (X = Br^-, I^- and SO_4^{2-}) and the basic principles can be applied to help rational synthesis of other high-yield metal NWs with tunable sizes.

1 Introduction

In recent years, silver nanowires (Ag NWs) have garnered considerable research attention because of their unique optical, mechanical, electrical, and thermal properties, [1–5] and have been extensively investigated as building blocks of flexible transparent conductive films (TCFs) [6–12]. Hence, the mass production of high-quality Ag NWs has evolved as an active research area during the past few decades. Of the various synthesis methods used for the preparation of Ag NWs, [1, 13–17] the polyol method [1, 13, 14]

Address correspondence to Liang Luo, luoliang@mail.buct.edu.cn; Yun Kuang, kuangyun@mail.buct.edu.cn

has been widely studied.

It is well known that Ag NWs possess a multi-twinned structure [14–17] with a pentagonal cross section, and the chemical potential (driving force) for the growth should be finely controlled since the twin defect means the highest energy site. Thus, the stabilization of the multi-twinned structure and keeping the precursor concentration low enough to avoid self-nucleation are key requirements for the preparation of Ag NWs. However, low precursor concentration results in lower utilization of solvent and surfactant, which in turn increases the cost of large-scale production of Ag NWs. This issue needs to be addressed for a facile large-scale production of Ag NWs with high concentration of Ag^+ in order to realize their practical applications.

Many efforts have been made to solve the above problem. A probable solution is to introduce noble metal nanoparticle seeds (e.g. Pt or Pd) to direct the growth of Ag NWs [1, 18]; however, the cost still remains high and the concentration increase of the resulting NWs is not guaranteed. Alternatively, introducing halide salts such as chloride (NaCl, $CuCl_2$) [19, 20] or bromide (NaBr) [21, 22] as heterogeneous nuclei to form AgX (X = Cl or Br), has been demonstrated to be an effective way to promote the formation of Ag NWs [16, 20, 23–27]. However, owing to the lack of a deep insight into heterogeneous nucleation processes, usually a trace amount of halide salts is added (<0.25 mM) [13, 19, 20]. Furthermore, the corresponding [Ag^+] has been found to be as low as 1.2 mM for aqueous systems and ~23 mM for polyol systems, thus rendering this approach impractical [13, 16]. Therefore, increasing the amount of the halide salt added while balancing the relationship with other parameters such as the precursor concentration, solvent, or reductant, has become a great challenge to program the growth behavior of Ag NWs, and it is therefore important to develop a rational approach for the facile and large-scale preparation of Ag NWs.

Herein, we investigated the concentration law of Cl^- in the hydrothermal synthesis of Ag NWs. Different amounts of Cl^- were introduced into the $AgNO_3$ solution with different concentrations to tune the molar ratio of Cl^-/Ag^+ in order to probe the growth mechanism of Ag NWs. A linear relationship between [Cl^-] and [Ag^+] was observed under optimized high-yield synthesis conditions. The trend could still be observed when the final Ag NW concentration was 5–20 times higher than that used traditionally in either aqueous or polyol systems. The strategy could also be successfully extended to polyol systems by using Cl^-, Br^-, I^-, and SO_4^{2-} ions. Besides, by tailoring heterogeneous nucleation sites, which is done by controlling the size of AgX seeds, the diameters of the final Ag NWs could be well controlled even in high concentration conditions. Thus, the synthetic strategy studied here can significantly lower the cost of the scaled-up production of Ag NWs, and the basic concept should motivate high yield mass production of similar metal NWs.

2 Experimental

2.1 Chemicals and materials

Silver nitrate (>99%), glucose (AR grade), anhydrous ethylene glycol (EG, 99.8%), polyvinylpyrrolidone (PVP) (AR grade, M_W ~ 58,000, PVP-58000), PVP-1300000 (AR grade, M_W ~ 1,300,000), sodium bromide (AR grade), sodium sulfate (AR grade), and sodium chloride (AR grade) were purchased from Beijing Chemical Reagents Company. Anhydrous ethanol (HPLC grade) and 18 MΩ deionized water were used as dispersion media. All reagents were used as-received without further purification.

2.2 Synthesis of silver nanowires by hydrothermal method

In a typical synthesis procedure, 1 g of glucose, 1 g of PVP-1300000, and 0.17 g of $AgNO_3$ were dissolved in 35 mL of deionized water to form a clear solution. 0.83 mL of 0.1 M NaCl solution in deionized water was added into the aforementioned mixture. Then the mixture was transferred to a 50 mL Teflon-sealed autoclave and heated at 140 ℃ for 18 h. Upon cooling to room temperature, the reaction mixture was washed thrice with deionized water. A final dispersion of Ag NWs in deionized water was thus obtained. In control experiments, we simply adjusted the addition amounts of $AgNO_3$ and NaCl, while maintaining the other conditions constant.

2.3 Synthesis of silver nanowires by polyol method

In a typical synthesis procedure, 6 mL of $AgNO_3$ solution (0.1 M in EG) and 3 mL of PVP-58000 solution (0.6 M in EG) were added rapidly into 14 mL of EG. Subsequently, 70 μL of NaCl solution (0.1 M in EG) was added slowly into the aforementioned mixture under stirring. The reaction was then performed at 140 ℃ for 1 h under stirring. Upon cooling to room temperature, the solutions were washed thrice with ethanol. A final dispersion of Ag NWs in deionized water was thus obtained. In the control experiments, we simply replaced NaCl solution with NaBr (0.1 M in EG), NaI (0.1 M in EG), and Na_2SO_4 (0.1 M in EG) solutions, while maintaining the other conditions constant.

3 Results and discussion

3.1 The optimized preparation of Ag NWs with hydrothermal method

We used aqueous-based synthesis of Ag NWs as a model system to investigate the multiple role of Cl^-. Glucose (1 g), polyvinylpyrrolidone (PVP-1300000, 1 g) [28] and $AgNO_3$ were used as the reductant, surfactant, and precursor, respectively. Figure 1(a) plots the relationship between the concentration of added Cl^- (NaCl) and the corresponding optimized [Ag^+] ($AgNO_3$). It should be noted that the yield of Ag NWs should be higher than 95% under "optimized" conditions after the repeated experiments. Due to a fast reaction between Ag^+ and Cl^- white precipitates were obtained when Cl^- was introduced to $AgNO_3$ solution before hydrothermal treatment. Digital photos (Fig. 1(a), inset) show three typical samples with low (5.7 mM Ag^+ and 0.14 mM Cl^-), medium (14 mM Ag^+ and 0.91 mM Cl^-), and high (28 mM Ag^+ and 2.36 mM Cl^-) concentrations, respectively. The amount of AgCl precipitates so obtained increased with an increase in the addition amount of Cl^-. Furthermore, the color of the AgCl precipitates became whiter as the addition amount of Cl^- increased. The solutions turned green after the reaction.

Figure 1(b) shows the UV–vis extinction spectra of the five obtained samples. All the samples show two characteristic surface plasmon resonance (SPR) peaks at 355 and 378 nm, indicating the formation of Ag NWs [1, 29]. Meanwhile, the sharp peaks indicate the

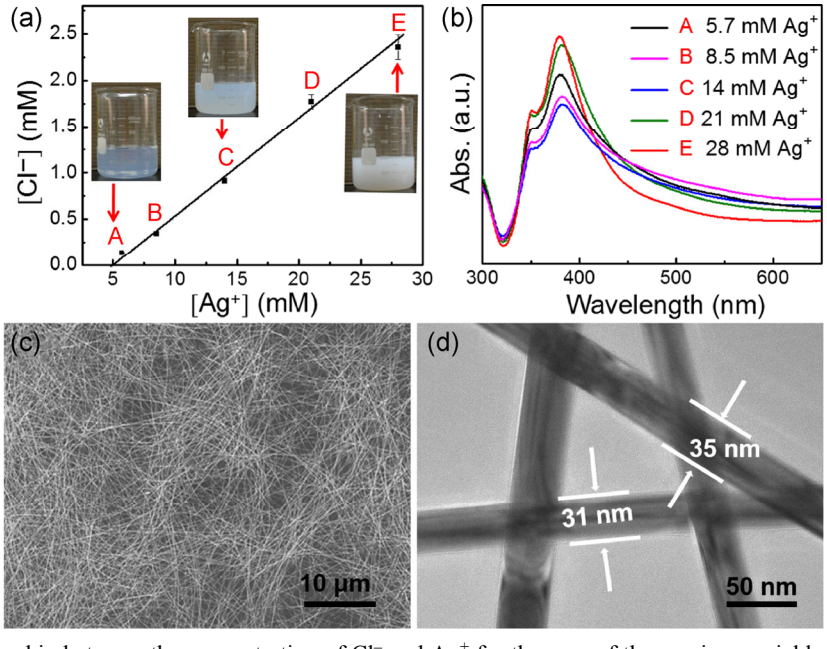

Figure 1 (a) The relationship between the concentration of Cl^- and Ag^+ for the case of the maximum yield of Ag NWs with different Ag^+ concentrations. Inset: photos of reaction solutions obtained by adding different amounts of Cl^- with different Ag^+ concentrations. (b) UV–vis spectra of Ag NWs prepared with different Ag^+ concentrations. (c) SEM image of Ag NWs. (d) Magnified TEM image of Ag NWs.

formation of high quality Ag NWs with few nanoparticles [1, 3]. The large-scale scanning electronic microscopy (SEM) image (Fig. 1(c)) of the sample (point E) prepared with a [Ag^+] of 28 mM confirmed the formation of high quality Ag NWs with a mean length of 60 ± 5 μm. The mean diameter of Ag NWs was found to be 33 ± 2 nm as observed from the magnified transmission electron microscopy (TEM) image (Fig. 1(d)). Hence, unlike "traditional" synthesis routes that use trace amounts Cl^- (0.25 mM) [16], the present method afforded Ag NWs in high-yield even when the aqueous phase concentration of Cl^- and Ag^+ ions was increased 9 and 20 times, respectively.

In order to investigate the relationship between the [Cl^-] added and [Ag^+] in the resulting NWs, we performed linear regression (Fig. 1(a), black line) for the experimental data as

$$[Cl^-] = a[Ag^+] + b \quad (1)$$

For the fitted line, R_2 was found to be 0.9921, indicating that the five points could be fit well to a linear relationship. The fitting parameters a and b were calculated to be 0.1032 and –0.488, respectively. As [Ag^+] and [Cl^-] followed a linear relationship, we could increase the concentration of Ag precursor ([Ag^+]) to synthesize Ag NWs by increasing [Cl^-] added and vice versa. For extremely low concentrations of Ag precursor, only a trace amount of Cl^- ions was introduced, which is in good accord with the "traditional" synthesis methods for the growth of multi-twinned Ag NWs [14–17]. Thus, a low chemical potential (driving force) could be maintained for the growth of Ag NWs at high [Ag^+] by increasing the amount of Cl^- ions added. The trend could not be further extended to even higher concentrations because the precursive AgCl precipitates would not be stable at these concentrations.

3.2 The growth behavior of Ag NWs

To investigate the role of the "large" amount of introduced Cl^- ions for the formation of highly concentrated Ag NWs, we monitored the initial nucleation and morphology evolution of Ag NWs synthesized using parameters of point E in Fig. 1(a) (28 mM Ag^+ and 2.36 mM Cl^-). Figure 2(a) shows the UV–Vis spectra

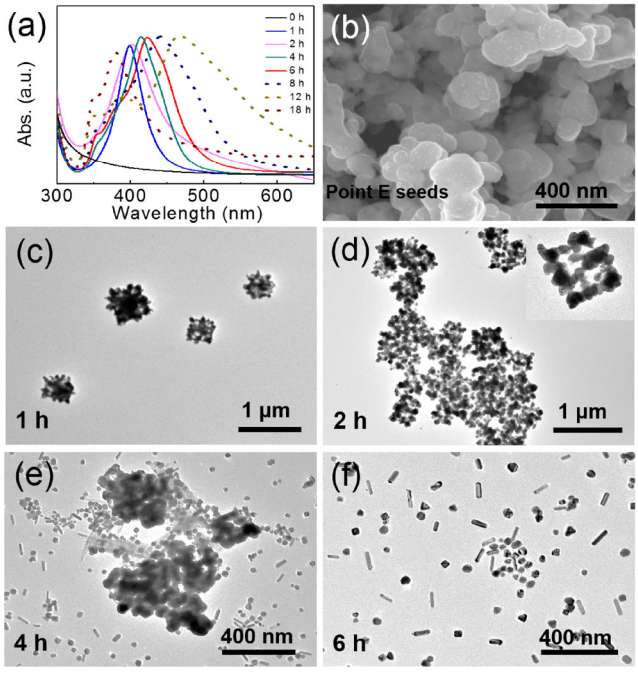

Figure 2 (a) UV–vis spectra of Ag nanostructures obtained after different reaction times. (b) SEM image of AgCl nanostructures at point E. (c)–(f) TEM images of Ag nanostructures obtained after the reaction times of 1, 2, 4, and 6 h.

of products obtained by varying the reaction time from 0 to 18 h. For the sample obtained after 0 h, only AgCl precipitate could be observed (Fig. 2(b)) without any characteristic peak of Ag nanostructures. As the reaction proceeded for 1 h, the characteristic peak of Ag nanoparticles at 398 nm appeared. TEM image (Fig. 2(c)) revealed that cube-like AgCl nanoparticles were obtained after [23, 30, 31] the hydrothermal treatment, and meanwhile, many tiny Ag nodules grew on the surface of AgCl-seeds, indicating the heterogeneous nucleation [23]. As the reaction time increased from 2 to 4 h, the Ag NPs gradually grew bigger on the surface of AgCl-seeds, which was confirmed by the slight red-shift of the characteristic peaks in the extinction spectra. The AgCl-seeds themselves tended to become hollow framed (Fig. 2(d), inset), and finally collapsed at 6 h, generating free Ag nanoparticles and short nanorods (Figs. 2(e) and 2(f)). As the reaction increased from 8 to 12 h, a significant increase in the number of nanorods was observed. Moreover, the extinction peak red-shifted from 439 to 466 nm (Fig. 2(a) and Fig. S1(a) in the Electronic Supplementary Material (ESM)) owing to the longitudinal SPR resulting from an increased aspect ratio

(Figs. S1(b)–S1(d) in the ESM) [1, 32]. After the reaction times of 14 h and more (Figs. S1(e)–S1(g) in the ESM), Ag nanorods rapidly grew longer to finally yield nanowires with constant diameter. The corresponding blue-shift in the extinction peak from 455 to 378 nm was observed, and finally the two characteristic SPR peaks (355 and 378 nm) of Ag NWs appeared (Fig. 2(a)).

The growth behavior of Ag NWs was further investigated by X-ray diffraction (XRD) measurements. As shown in Fig. 3(a), five typical samples obtained at 1, 4, 6, 12 and 18 h, respectively were tested. The intensity of the strong characteristic peaks indexing to (111), (200), and (220) planes of AgCl [23, 26] gradually decreased as the reaction time increased from 1 to 6 h, which dramatically decreased after 6 h. This is in good agreement with the observation of the collapse of AgCl-seeds from TEM images (Fig. 2(f)), possibly because dissolve/precipitation equilibrium converted the AgCl particles to very tiny amorphous species. After the reaction time of 4 h, the Ag nodules grew bigger in size enough, which was confirmed by the appearance of the characteristic XRD peaks for (111) and (200) planes of cubic phased Ag. The typical intensity ratio of (111)/(200) for Ag NWs is 3:1:1. The intensity ratio of (111)/(200) for our samples obtained after 4 h varied from 1:2.8 to 3.1:1, which is due to the morphological evolution from Ag nanoparticles to nanowires. Enrichment of {111} crystalline planes in the Ag NWs was thus confirmed (Fig. 3(a) and Fig. S2 in the ESM) [1, 20].

Furthermore, the kinetics of growth was also investigated by the inductive coupled plasma emission spectrometer (ICP) analysis for the residual [Ag^+] during the growth, and the length of the obtained products was revealed by SEM/TEM images (Fig. 3(b)). We divided the entire growth procedure into three stages: 1) nucleation, 2) growth of nanorods, and 3) growth of nanowires, as shown in Fig. 3(b). The first stage (0–6 h) started with a rapid heterogeneous nucleation process. Many tiny Ag nodules grew on the surface of the AgCl nanoparticles and served as nuclei. Then the freshly reduced Ag^0 atoms subsequently deposited on the tiny Ag nodules and spread into solution after the collapse of AgCl seeds. [Ag^+] decreased rapidly, indicating a quick nucleation at this stage. In the second stage (6–12 h), some multi-twinned rod-shaped Ag nanoparticles gradually formed with an increase in length limited to several hundred nanometers, which can be observed from SEM images (Figs. S1(b) and S1(c) in the ESM) or the magnified TEM image (Fig. S1(d) in the ESM, inset) thus leaving single crystalline nanoparticles essentially unchanged in the solution. During this stage, some fusion and dissolution of tiny Ag nanoparticles was also observed, and correspondingly the consumption rate of Ag^+ was relatively slow. The third stage (12–18 h) was marked by a significant increase in the length of the nanorods accompanied by a rapid consumption of the remaining Ag^+ species (ca. 56%), which thus resulted in the formation of Ag NWs with a mean length of 60 μm. Moreover, the length could be extended by further addition of the Ag precursor ([Ag^+]) during the growth stage [19, 33]. The heterogeneous nucleation and growth process are summarized in Scheme 1. Buhro et al. have carefully investigated the heterogeneous nucleation of Ag nuclei on the surface of micron-sized AgCl particles and their observations further confirmed the model [23].

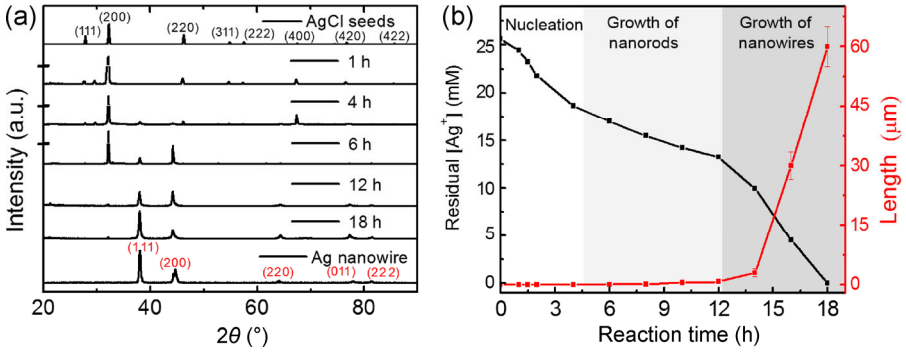

Figure 3 (a) XRD patterns of the Ag nanostructures obtained after *t* different reaction times. (b) The relationship between the reaction time and the residual concentration of Ag^+ and the length of Ag NWs.

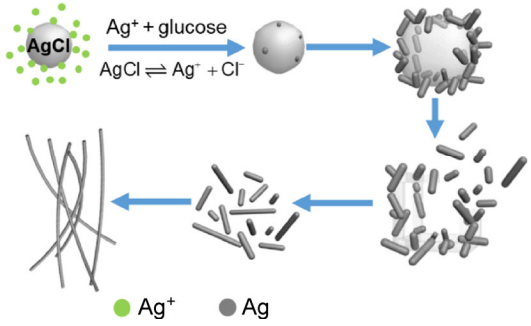

Scheme 1 Schematic of the heterogeneous nucleation and growth of Ag NWs with high concentration of Ag^+ by introducing large amount of Cl^- ions.

3.3 The proposed mechanism for the growth of Ag NWs

In light of our observations on the growth of Ag NWs, the role of Cl^- ions can be understood by the following mechanism: First, since the Ag^+ ions are in excess as compared to the Cl^- ions, the free Ag^+ ions were adsorbed on the surface of AgCl colloid nanoparticles, as evidenced by the positive potential of AgCl nanoparticles in Fig. S3 (in the ESM). Such adsorption on the colloid surface can be regarded as a kind of enrichment to form locally high Ag^+ concentration and thus make the surface more active for reduction. Also, the solid–liquid interfaces of colloids provided ideal heterogeneous nucleation sites for the resultant Ag after reduction. Second, since the heterogeneous nucleation occurred at the surface of the well dispersed AgCl-seeds, the growth sites were well scattered, and the steric effect also helped to prevent the aggregation of the resultant Ag nuclei, which could happen without AgCl in the solution with such a high [Ag^+]. During the second NW growth stage (6–12 h), the AgCl nanoparticles still existed in the solution as tiny amorphous species rather than getting converted to Ag^0, which was further evidenced by the mismatched distribution of Cl and Ag in the energy-dispersive X-ray spectra (EDS, Fig. S4 in the ESM) of the products obtained after 6 and 12 h and the disappearance of the peaks for AgCl in the XRD spectra of the same (Fig. 3(a)).

3.4 Size evolution of AgCl colloids

It is worth noting that, owing to the relatively weak reducibility of glucose (as the reductant for the study of aqueous phase here) at 140 ˚C, AgCl could not be directly reduced to Ag^0, which was confirmed from the same XRD patterns obtained before and after the hydrothermal treatment of the mixture of AgCl and glucose. SEM image of the product also confirmed the same (Fig. S5 in the ESM). Hence, we can say that the AgCl nanoparticles served as nuclei here.

Given that the AgCl-seeds supported the heterogeneous nucleation, we tried to elucidate the linear relationship between [Ag^+] and [Cl^-]. We believe that the key to balance the two concentrations was the total surface area of the AgCl nanoparticles, which in turn depended on the size and number of AgCl-seeds. Interestingly, the results indicated that the size of the individual AgCl-seeds did not increase much with the concentration. As we demonstrated using SEM, all the AgCl-seeds obtained by five points (A–E in Fig. 1(a)) formed cube-like structures (Fig. S6 in the ESM) with relative uniformity. Dynamic light scattering (DLS) measurement (Fig. S7 in the ESM) showed that the diameter of the AgCl-seeds from remained almost constant from point A to point D, indicating a constant relative size distribution for AgCl colloid suspension (Fig. 4(a)). For the threshold value of the introduced [Cl^-] at point E, there was an obvious increase in the diameter of the obtained AgCl-seeds, probably due to slight aggregation. The slight aggregates were de-aggregated in the subsequent hydrothermal reaction. Thus the total surface area was proportional to the total aggregate amount, i.e. the total concentration of Cl^- ions. For the growth of high-quality Ag NWs with different Ag^+ concentrations, the number of nucleation sites (i.e. total surface area) should increase with the same ratio to scatter the nucleation and growth behaviors. Hence, the surface area (S_{AgCl}) and volume (V_{AgCl}) of the individual AgCl-seeds remained relatively stable in an appropriate range of [Cl^-] (0–2.3 mM, points A–E) and the number of AgCl-seeds (N_{AgCl}) increased linearly with the introduction of Cl^- (Fig. 4(b)). We believe that this is the reason why the introduced [Cl^-] versus the corresponding [Ag^+] had a perfect linear relationship for the preparation of Ag NWs (Fig. 1(a)). The underlying mechanism was the linear relationship between the concentration of Ag^+ ions and the number of growth sites.

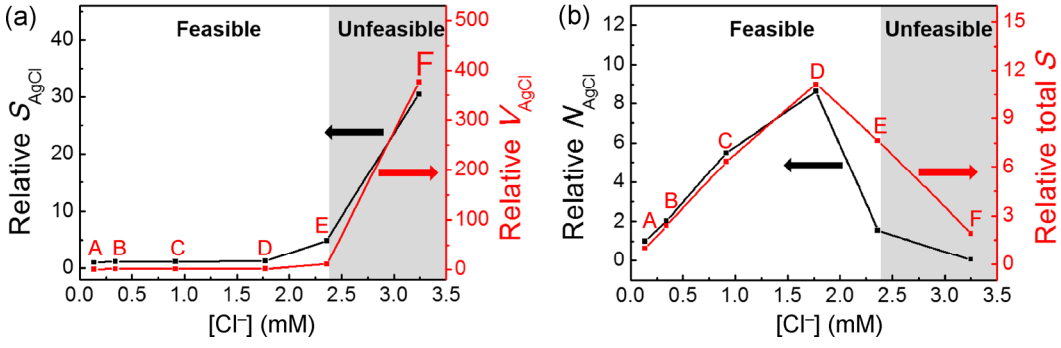

Figure 4 Calculation of AgCl seeds based on DLS data. (a) The relative S_{AgCl} and V_{AgCl} of single AgCl-seeds at different Cl^- concentrations. (b) The relative N_{AgCl} and total surface area of AgCl-seeds at different Cl^- concentrations.

3.5 The growth behavior of Ag NWs with saturated [Cl^-]

As a support to our proposal, we noticed that, if too high [Cl^-] (3.2 mM, denoted as point F) was introduced, there would be some inevitable micron-sized aggregation of the AgCl precipitates (Fig. S7(f) in the ESM) [23], which would largely decrease the total surface area (Fig. 4(b)), thus decreasing the number of the available nucleation sites. As supported by SEM image (Fig. 5(a)), the obtained product was the mixture of Ag nanoparticles, Ag nanowires, and micron-sized AgCl particles. The strong characteristic XRD peaks of AgCl (200) in the XRD patterns of the obtained products confirmed the existence of AgCl as big particles in the final product of point F apart from the tiny amorphous particles in the final product of point E (marked as red circle in Fig. 5(b)), which was further evidenced by the SEM image and the well-matched distribution of Cl and Ag in the EDS spectra (Fig. 5(c)). As a result, for the preparation of Ag NWs with higher [Cl^-] (point F), on one hand, the total surface area of the micron-sized AgCl-seeds dramatically decreased, which broke the stable ratio of [Ag^+]/[Cl^-] and disturbed the heterogeneous nucleation; on the other hand, the "unbreakable" micron-sized AgCl-

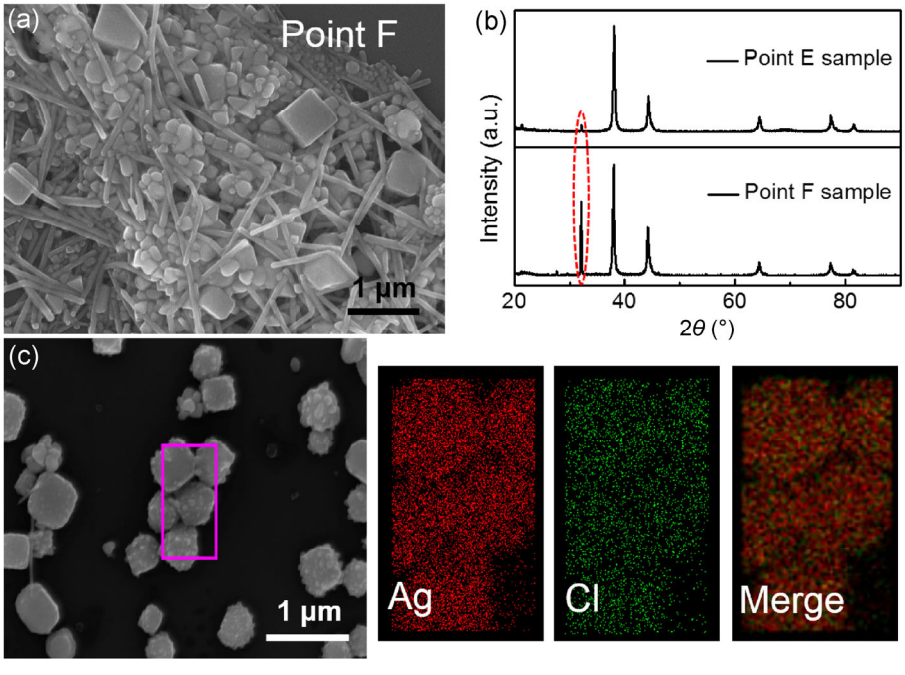

Figure 5 (a) SEM image of the product of point F. (b) XRD patterns of product of points E and F. (c) EDS of the precipitation of the product of point F.

seeds would still adsorb Ag^+ and compete with the detached free Ag^0 seeds during the growth stage. Therefore, the high-concentration preparation of Ag NWs should be realized by introducing Cl^- ions in an appropriate concentration range (marked as "feasible zone" in Fig. 4), where the chemical potential could be finely controlled by the surface area of the AgCl-seeds increasing linearly (nucleation sites) with $[Ag^+]$.

3.6 The optimized preparation of Ag NWs with polyol method

In this context, with the aim to achieve a deterministic control on the preparation of Ag NWs at a large scale, the two values of a and b in Eq. (1), corresponding to the slope and intercept of the linear relationship, respectively, should be highly concerned. It is well-known that the fine control of the chemical potential (driving force) plays a very important role in the nucleation of the multi-twinned structures. Technically, the chemical potential is mainly determined by the reaction temperature, precursor (resource of Ag^+), reductant, and the nucleation sites. Here in this study, the reaction temperature was 140 °C, and $AgNO_3$ and glucose acted as the precursor and reductant, respectively. The only variable was the nucleation sites, which were determined by the amount of Cl^- introduced. With the understanding of the linear relationship between $[Ag^+]$ and $[Cl^-]$, the value of the slope (0.1032) (corresponding to a) was determined by the size of the AgCl colloids in the solution. According to the fitted line, if no Cl^- was added, Ag NWs could be prepared with a $[Ag^+]$ as low as 4.7 mM (corresponding to b), which was consistent with the results of previously reported studies [16, 34, 35]. Hence, as no heterogeneous nucleation occurred, the intercept (corresponding to b) is thereby determined by the chemical potential, which depends on other factors namely, the type and concentration of precursor, reaction temperature, and reductant.

3.7 The preparation of Ag NWs with AgX-seeds

For further investigation of the magnified heterogeneous nucleation induced preparation of Ag NWs, we extended the synthesis to polyol system. Typically, $AgNO_3$ and PVP solution were added rapidly into EG and 70 μL NaCl solution (0.1 M in EG) was added into the mixture under stirring. Then the reaction was performed at 140 °C for 1 h under stirring. Figure 6(a) shows the relationship between the concentration of added Cl^- and Ag for obtaining high-quality Ag NWs. It was revealed that the precipitation behavior of AgCl in EG in the polyol system was the same as that in the aqueous system. The slope (a) and the intercept (b) for the polyol system were 0.021 and –0.2098 (R_2 is 0.9962), respectively. Due to the relatively higher reducibility of EG, we could prepare Ag NWs with $[Ag^+]$ of 10 mM without adding any Cl^-, which is higher than that (4.7 mM) in the aqueous system. With the introduction of Cl^-, $[Ag^+]$ could be increased to a value as high as 130 mM, which was 5 times higher than the previously reported value thus confirming the successful extension of our strategy to polyol synthesis of Ag NWs (Fig. 6(b)).

An alternative is to replace Cl^- with other anions such as Br^-, I^-, and SO_4^{2-}. Control experiments were conducted to prepare Ag NWs using the polyol method. As revealed by SEM (Fig. S8 in the ESM), the average size of the as-formed precipitated colloids was in the range 800–3,000 nm for Ag_2SO_4, 115–300 nm for AgCl, 110–180 nm for AgBr, and 80–135 nm for AgI. The size thus decreased in the following trend: $SO_4^{2-} > Cl^- > Br^- > I^-$, which is in accordance with the solubility order of AgX (see the ESM) [36, 37], and essentially the same trend as the amount except SO_4^{2-} owing to the valance state of –2. Figure S9 in the ESM shows the extinction spectra of the four products prepared with the same $[Ag^+]$. The typical peak shapes verified the successful synthesis of Ag NWs. With the understanding of the

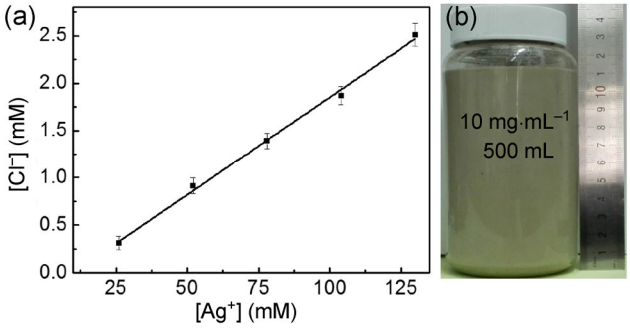

Figure 6 (a) The relationship between the Cl^- and Ag^+ concentrations for the preparation of Ag NWs in the polyol system. (b) Digital photo of the obtained Ag NWs for one pot.

magnified heterogeneous nucleation induced preparation of Ag NWs, we believe that the length and the diameter of the as-prepared Ag NWs could be tuned using different anions. Owing to the smallest average size, the total surface area of the AgI-seeds should be the largest and should have the highest number of nucleation sites. The smallest AgI-seeds could least sustain the growth of Ag nodules on the surface, which directly determines the diameter of the Ag NWs. Thus, the thinnest Ag NWs were obtained with I^- under the same precursor [Ag^+], and vice versa. The Ag NWs prepared with SO_4^{2-} should be the thickest. As supported by the SEM images (Fig. 7), the diameters of the Ag NWs prepared by adding SO_4^{2-}, Cl^-, Br^-, and I^- were 62–89, 63–68, 51–53, and 36–38 nm, respectively; and the lengths were 35–40, 10–15, 6–10, and 5–6 μm, respectively. The related information is summarized in Table 1. As a result, it was verified that the diameter of the Ag NWs could be tuned by introducing different anions.

Therefore, the control experiments confirmed that the major and important role of AgX precipitates was to provide abundant surface area for the heterogeneous nucleation of the Ag NWs at high [Ag^+] thus effectively lowering the chemical potential. Ag NWs are generally prepared on a large scale by the introduction of different anions and adjusting their unique precipitation behavior with high [Ag^+]. In addition, it can be concluded that several aspects determining the optimized synthesis of high-concentration Ag NWs are: 1) nucleation stage: introducing one or multiple anions [38] to form AgX-seeds as small as possible with low solubility such as I^-; or introducing poor solvents to reduce the solubility of the AgX-seeds [36, 37]; 2) growth stage: Further addition of $AgNO_3$ may help to extend the growth of NWs [19, 33].

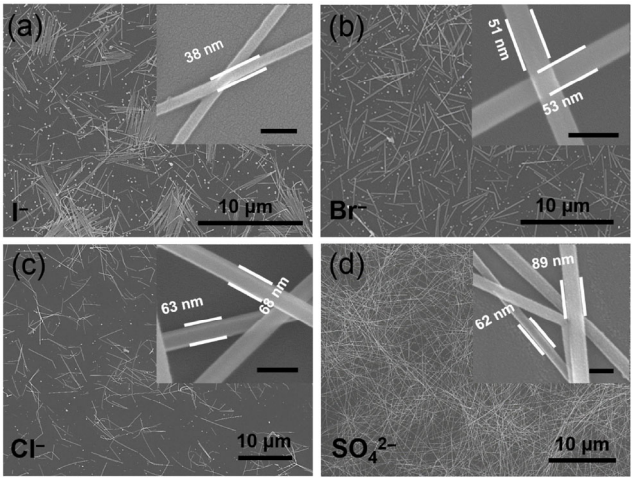

Figure 7 SEM images of Ag NWs prepared by adding (a) I^-, (b) Br^-, (c) Cl^- and (d) SO_4^{2-}. Inset: the magnified SEM images for the Ag NWs, the scale bars are at 100 nm.

Table 1 The related information of Ag NWs and seeds in polyol system

Seeds	AgI	AgBr	AgCl	Ag_2SO_4
Concentration of seeds (mM)	0.196	0.239	0.304	0.175
Size of seeds (nm)	80–135	110–180	115–300	800–3,000
Diameter of Ag NWs (nm)	36–38	51–53	63–68	62–89
Length of Ag NWs (μm)	5–6	6–10	10–15	35–40

For the demonstration of the application of Ag NWs, we prepared TCFs by Meyer-rod coating the Ag NW (5 mg·mL^{-1}, dispersed in water) inks on flexible PET substrates (Fig. S10 in the ESM). The sheet resistance could reach (65 ± 3) Ω·sq^{-1} (SO_4^{2-}), (100 ± 5) Ω·sq^{-1} (Cl^-), (160 ± 10) Ω·sq^{-1} (Br^-), and (200 ± 10) Ω·sq^{-1} (I^-), and the transparency at 550 nm could reach values of 96.18%, 83.52%, 79.96%, and 71.11% as the length of Ag NWs decreased. The lowest sheet resistance and the best transparency of TCFs were achieved for the Ag NWs prepared with SO_4^{2-}. The high quality of the as-prepared Ag NWs was attributed to the lowest wire-wire junction resistance.

4 Conclusions

In conclusion, we developed a general and facile synthetic strategy for large-scale production of high-concentration Ag NWs by increasing the feeding amount of Cl^-. Owing to the essentially stable size of AgCl colloids, the feeding amount of [Cl^-] versus [Ag^+] shows a linear trend in both aqueous and polyol systems, which is the key factor for the heterogeneous nucleation during Ag NW growth. The strategy was also successfully extended to the polyol system with Cl^-, Br^-, I^-, and SO_4^{2-} ions. With the new synthetic approach, the cost of the large-scale production of Ag NWs can be significantly lowered, and the basic

concept should motivate high yield production of similar metal NWs.

Acknowledgements

This work was support by the National Natural Science Foundation of China, the Program for Changjiang Scholars and Innovative Research Team in the University, and the Fundamental Research Funds for the Central Universities, and the long-term subsidy mechanism from the Ministry of Finance and the Ministry of Education of PRC.

Electronic Supplementary Material: Supplementary material (additional characterization data of SEM/TEM images, optical images, EDS, XRD, and DLS) is available in the online version of this article at http://dx.doi.org/10.1007/s12274-016-1049-2.

References

[1] Sun, Y. G.; Yin, Y. D.; Mayers, B. T.; Herricks, T.; Xia, Y. N. Uniform silver nanowires synthesis by reducing $AgNO_3$ with ethylene glycol in the presence of seeds and poly(vinyl pyrrolidone). *Chem. Mater.* **2002**, *14*, 4736–4745.

[2] Rycenga, M.; Cobley, C. M.; Zeng, J.; Li, W. Y.; Moran, C. H.; Zhang, Q.; Qin, D.; Xia, Y. N. Controlling the synthesis and assembly of silver nanostructures for plasmonic applications. *Chem. Rev.* **2011**, *111*, 3669–3712.

[3] Xia, Y. N.; Xiong, Y. J.; Lim, B.; Skrabalak, S. E. Shape-controlled synthesis of metal nanocrystals: Simple chemistry meets complex physics? *Angew. Chem., Int. Ed.* **2009**, *48*, 60–103.

[4] Stewart, M. E.; Anderton, C. R.; Thompson, L. B.; Maria, J.; Gray, S. K.; Rogers, J. A.; Nuzzo, R. G. Nanostructured plasmonic sensors. *Chem. Rev*. **2008**, *108*, 494–521.

[5] Halas, N. J.; Lal, S.; Chang, W. S.; Link, S.; Nordlander, P. Plasmons in strongly coupled metallic nanostructures. *Chem. Rev.* **2011**, *111*, 3913–3961.

[6] Zhu, R.; Chung, C. H.; Cha, K. C.; Yang, W. B.; Zheng, Y. B.; Zhou, H. P.; Song, T. B.; Chen, C. C.; Weiss, P. S.; Li, G. et al. Fused silver nanowires with metal oxide nanoparticles and organic polymers for highly transparent conductors. *ACS Nano* **2011**, *5*, 9877–9882.

[7] Ye, S. R.; Rathmell, A. R.; Chen, Z. F.; Stewart, I. E.; Wiley, B. J. Metal nanowire networks: The next generation of transparent conductors. *Adv. Mater*. **2014**, *26*, 6670–6687.

[8] Madaria, A. R.; Kumar, A.; Ishikawa, F. N.; Zhou, C. W. Uniform, highly conductive, and patterned transparent films of a percolating silver nanowire network on rigid and flexible substrates using a dry transfer technique. *Nano Res*. **2010**, *3*, 564–573.

[9] Liang, J. J.; Li, L.; Niu, X. F.; Yu, Z. B.; Pei, Q. B. Elastomeric polymer light-emitting devices and displays. *Nat. Photonics* **2013**, *7*, 817–824.

[10] Wu, H.; Kong, D. S.; Ruan, Z. C.; Hsu, P. C.; Wang, S.; Yu, Z. F.; Carney, T. J.; Hu, L. B.; Fan, S. H.; Cui, Y. A transparent electrode based on a metal nanotrough network. *Nat. Nanotechnol.* **2013**, *8*, 421–425.

[11] Zeng, X. Y.; Zhang, Q. K.; Yu, R. M.; Lu, C. Z. A new transparent conductor: Silver nanowire film buried at the surface of a transparent polymer. *Adv. Mater.* **2010**, *22*, 4484–4488.

[12] Tao, A.; Kim, F.; Hess, C.; Goldberger, J.; He, R. R.; Sun, Y. G.; Xia, Y. N.; Yang, P. D. Langmuir-Blodgett silver nanowire monolayers for molecular sensing using surface-enhanced Raman spectroscopy. *Nano Lett*. **2003**, *3*, 1229–1233.

[13] Sun, Y. G.; Gates, B.; Mayers, B.; Xia, Y. N. Crystalline silver nanowires by soft solution processing. *Nano Lett*. **2002**, *2*, 165–168.

[14] Sun, Y. G.; Mayers, B.; Herricks, T.; Xia, Y. N. Polyol synthesis of uniform silver nanowires: A plausible growth mechanism and the supporting evidence. *Nano Lett*. **2003**, *3*, 955–960.

[15] Wiley, B.; Herricks, T.; Sun, Y. G.; Xia, Y. N. Polyol synthesis of silver nanoparticles: Use of chloride and oxygen to promote the formation of single-crystal, truncated cubes and tetrahedrons. *Nano Lett*. **2004**, *4*, 1733–1739.

[16] Sun, X. M.; Li, Y. D. Cylindrical silver nanowires: Preparation, structure, and optical properties. *Adv. Mater*. **2005**, *17*, 2626–2630.

[17] Sun, Y. G.; Ren, Y.; Liu, Y. Z.; Wen, J. G.; Okasinski, J. S.; Miller, D. J. Ambient-stable tetragonal phase in silver nanostructures. *Nat. Commun*. **2012**, *3*, 971.

[18] Luo, M.; Huang, H. W.; Choi, S. I.; Zhang, C.; da Silva, R. R.; Peng, H. C.; Li, Z. Y.; Liu, J. Y.; He, Z. K.; Xia, Y. N. Facile synthesis of Ag nanorods with no plasmon resonance peak in the visible region by using Pd decahedra of 16 nm in size as seeds. *ACS Nano* **2015**, *9*, 10523–10532.

[19] Korte, K. E.; Skrabalak, S. E.; Xia, Y. N. Rapid synthesis of silver nanowires through a $CuCl^-$ or $CuCl^{2-}$ mediated polyol process. *J. Mater. Chem*. **2008**, *18*, 437–441.

[20] Gou, L. F.; Chipara, M.; Zaleski, J. M. Convenient, rapid synthesis of Ag nanowires. *Chem. Mater*. **2007**, *19*, 1755–1760.

[21] Ran, Y. X.; He, W. W.; Wang, K.; Ji, S. L.; Ye, C. H. A one-step route to Ag nanowires with a diameter below 40 nm and an aspect ratio above 1000. *Chem. Commun*. **2014**, *50*, 14877–14880.

[22] Hu, L. B.; Kim, H. S.; Lee, J.-Y.; Peumans, P.; Cui, Y. Scalable coating and properties of transparent, flexible, silver nanowire electrodes. *ACS Nano* **2010**, *4*, 2955–2963.

[23] Schuette, W. M.; Buhro, W. E. Silver chloride as a heterogeneous nucleant for the growth of silver nanowires. *ACS Nano* **2013**, *7*, 3844–3853.

[24] Liu, S.; Yue, J.; Gedanken, A. Synthesis of long silver nanowires from AgBr nanocrystals. *Adv. Mater*. **2001**, *13*, 656–658.

[25] Wang, Z. H.; Liu, J. W.; Chen, X. Y.; Wan, J. X.; Qian, Y. T. A simple hydrothermal route to large-scale synthesis of uniform silver nanowires. *Chem.—Eur. J.* **2005**, *11*, 160–163.

[26] Tetsumoto, T.; Gotoh, Y.; Ishiwatari, T. Mechanistic studies on the formation of silver nanowires by a hydrothermal method. *J. Colloid Interface Sci*. **2011**, *362*, 267–273.

[27] Im, S. H.; Lee, Y. T.; Wiley, B.; Xia, Y. N. Large-scale synthesis of silver nanocubes: The role of HCl in promoting cube perfection and monodispersity. *Angew. Chem.* **2005**, *117*, 2192–2195.

[28] Zhu, J. J.; Kan, C. X.; Wan, J. G.; Han, M.; Wang, G. H. High-yield synthesis of uniform Ag nanowires with high aspect ratios by introducing the long-chain PVP in an improved polyol process. *J. Nanomater.* **2011**, *2011*, Article ID 982547.

[29] Wiley, B. J.; Chen, Y.; McLellan, J. M.; Xiong, Y. J.; Li, Z. Y.; Ginger, D.; Xia, Y. N. Synthesis and optical properties of silver nanobars and nanorice. *Nano Lett*. **2007**, *7*, 1032–1036.

[30] Tang, Y. X.; Jiang, Z. L.; Xing, G. C.; Li, A. R.; Kanhere, P. D.; Zhang, Y. Y.; Sum, T. C.; Li, S. Z.; Chen, X. D.; Dong, Z. L. et al. Efficient Ag@AgCl cubic cage photocatalysts profit from ultrafast plasmon-induced electron transfer processes. *Adv. Funct. Mater*. **2013**, *23*, 2932–2940.

[31] Lou, Z. Z.; Huang, B. B.; Qin, X. Y.; Zhang, X. Y.; Cheng, H. F.; Liu, Y. Y.; Wang, S. Y.; Wang, J. P.; Dai, Y. One-step synthesis of AgCl concave cubes by preferential overgrowth along <111> and <110> directions. *Chem. Commun*. **2012**, *48*, 3488–3490.

[32] Link, S.; El-Sayed, M. A. Spectral properties and relaxation dynamics of surface plasmon electronic oscillations in gold and silver nanodots and nanorods. *J. Phys. Chem. B* **1999**, *103*, 8410–8426.

[33] Lee, J. H.; Lee, P.; Lee, D.; Lee, S. S.; Ko, S. H. Large-scale synthesis and characterization of very long silver nanowires via successive multistep growth. *Cryst. Growth Des.* **2012**, *12*, 5598–5605.

[34] Yang, Z. Q.; Qian, H. J.; Chen, H. Y.; Anker, J. N. One-pot hydrothermal synthesis of silver nanowires via citrate reduction. *J. Colloid Interface Sci*. **2010**, *352*, 285–291.

[35] Xu, J.; Hu, J.; Peng, C. J.; Liu, H. L.; Hu, Y. A simple approach to the synthesis of silver nanowires by hydrothermal process in the presence of gemini surfactant. *J. Colloid Interface Sci.* **2006**, *298*, 689–693.

[36] Xu, X. X.; Zhuang, J.; Wang, X. SnO_2 quantum dots and quantum wires: Controllable synthesis, self-assembled 2D architectures, and gas-sensing properties. *J. Am. Chem. Soc.* **2008**, *130*, 12527–12535.

[37] Hu, S.; Wang, X. Ultrathin nanostructures: Smaller size with new phenomena. *Chem. Soc. Rev*. **2013**, *42*, 5577–5594.

[38] Li, B.; Ye, S. R.; Stewart, I. E.; Alvarez, S.; Wiley, B. J. Synthesis and purification of silver nanowires to make conducting films with a transmittance of 99%. *Nano Lett*. **2015**, *15*, 6722–6726.